Post-Newtonian SPH Simulations of Binary Neutron Stars

Joshua A. Faber and Frederic A. Rasio

Department of Physics, M.I.T., 77 Massachusetts Ave., Cambridge, MA 02139

Abstract. Using our Post-Newtonian SPH (smoothed particle hydrodynamics) code, we study the final coalescence and merging of neutron star (NS) binaries. We find that the gravity wave signals can be computed accurately for irrotational systems in calculations of sufficient resolution, even in the presence of Kelvin-Helmholtz instabilities.

INTRODUCTION

Coalescing binary neutron stars (NS) are among the most promising sources of gravitational radiation that should be detectable by future generations of gravity wave detectors. LIGO, VIRGO, GEO, and TAMA may ultimately not only serve to test the predictions of the theory of general relativity (GR), but could also yield important information on the interior structure of neutron stars, which cannot be obtained directly in any other way.

Essentially all recent calculations agree on the basic picture that emerges during the final coalescence (see [1] and [2] for a complete list of references). As the binary approaches the dynamical stability limit, located at separations of $r = 3-4R_{NS}$, the NS plunge together rapidly and merge within a few rotation period. Mass shedding typically commences immediately after first contact, especially for initially synchronized systems. This material forms a pair of spiral arms before dissipating to form a dusty torus around the merger remnant. For stiff equations of state (EOS), the merger remnant can support a long-lived ellipsoidal (triaxial) deformation, which will radiate a significant level of gravity waves well after the merger is completed. Softer EOS relax toward spheroidal, non-radiating configurations on a dynamical timescale.

Of course, all statements about merger remnants assume that the remnant formed does not immediately collapse to a black hole (BH). Unfortunately Newtonian simulations are incapable of demonstrating such an effect. Instead, Newtonian calculations, using both Eulerian, grid based codes [3–9], and particle-based SPH methods [10–14], have studied many aspects of coalescing binaries, including the dependence of gravity wave signals on the initial spins, binary mass ratio, and NS EOS. Unfortunately, Newtonian gravity is a poor approximation to the physical situation

CP586, *Relativistic Astrophysics: 20th Texas Symposium,* edited by J. C. Wheeler and H. Martel

being studied. NS have extremely deep gravitational potentials, especially in their cores, even for very stiff EOS, and reach relativistic speeds during coalescence. Thus, proper treatment of the problem requires taking into account GR effects. Perhaps the most important effect of general relativity is to change the location of the dynamical stability limit, since relativistic corrections, even when small, can greatly affect the location of the minimum equilibrium energy E_{equil} as a function of separation, altering the point at which the binary begins its final rapid plunge toward merger.

Several groups have been working on full GR calculations [15], but only preliminary results have been reported so far. Extracting waveforms from the boundaries of grids has proves to be particlarly difficult. The middle ground between Newtonian calculations and full GR lies with PN hydrodynamics treatments. We [1,16], as well as Ayal et al. [17], have constructed a PN SPH code to calculate binary mergers. Our code uses the formalism of Blanchet, Damour, and Schaefer [18], adapted to a Lagrangian SPH framework. While it has proven impossible to include full-strength first-order (1PN) relativistic corrections, since they are often of comparable magnitude to Newtonian quantities for realistic NS parameters, we have devised a formalism whereby 1PN corrections are treated at reduced strength, while radiation reaction effects (2.5PN) are included at their physical values. This formalism is described in detail in [16].

IRROTATIONAL BINARY COALESCENCE

Our most detailed calculation performed to date uses $N = 500,000$ particles per NS, corresponding to the highest spatial resolution ever for a binary coalescence calculation. The calculation was performed using an irrotational initial condition. This is generally thought to be the most realistic case since the viscous tidal locking timescale for two NS is expected to be considerably longer than the inspiral timescale [19]. We model the initial density and velocity profile of the NS as tidally stretched ellipsoids, with parameters drawn from the PN equlibrium calculations of Lombardi, Rasio, and Shapiro [20]. We choose equal mass NS, and use a $\Gamma = 3$ polytropic EOS. Particle plots showing the evolution of the equal-mass irrotational binary system are shown in Fig. 1.

Immediately prior to merger, we see that a large tidal lag angle develops, as the inner edge of each NS leads the axis connecting the respective centers of mass, with the outer regions lagging behind. This is seen in Newtonian calculations, but is greatly enhanced by the addition of 1PN terms. Unlike the standard results from synchronized calculations, we do not see significant mass shedding from the system. The rotational speed of particles on the outer half of each NS is reduced in the irrotational case with respect to the synchronized case, and such particles are never ejected. The amount of mass shed is extremely small, much less than 1% of the total mass, and the velocities of the particles ejected are not sufficient to escape the gravitational potential of the remnant.

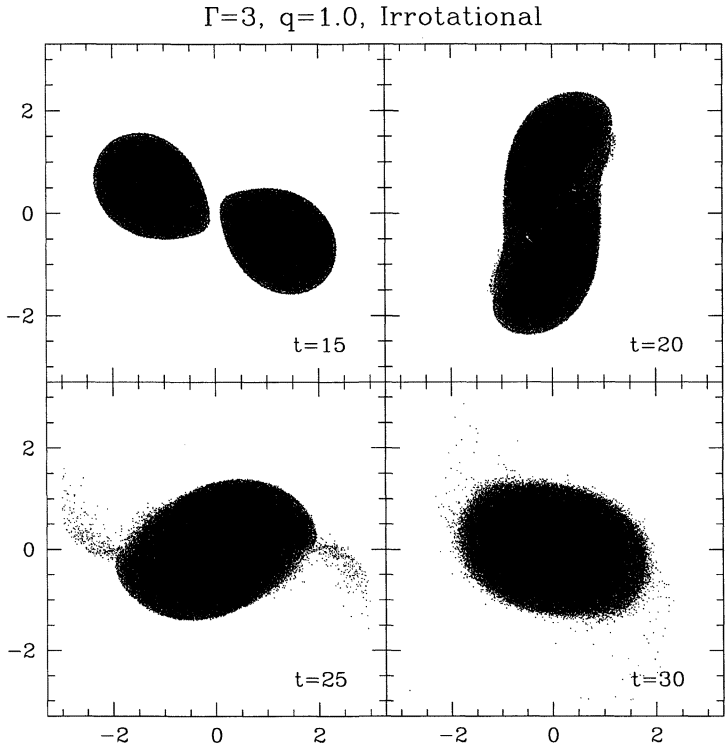

FIGURE 1. Final merger of two identical $\Gamma = 3$ polytropes with an irrotational initial condition. SPH particles are projected onto the equatorial plane of the binary. The orbital rotation is counterclockwise. Spatial coordinates are given in units of the NS radius R. Times are given in units of the dynamical timescale of the system, which here is $t_D = 0.07\text{ms} = 1$.

Density contours and velocity profiles in the equatorial plane of the binary are shown in Fig. 2. Velocities are shown in a frame corotating with the material, which highlights the Kelvin-Helmholtz unstable vortex sheet which forms along the surface of contact between the two NS. Large vortices form along this sheet, mixing material from the two NS, from $t = 20 - 25$. However, during this time the respective NS cores continue to inspiral toward the center of the forming remnant, until by $t = 30$ they have merged to form a single core, the vortices having merged together as well. This produces a characteristic differential rotation pattern, with the core spinning approximately twice as fast as the outer regions.

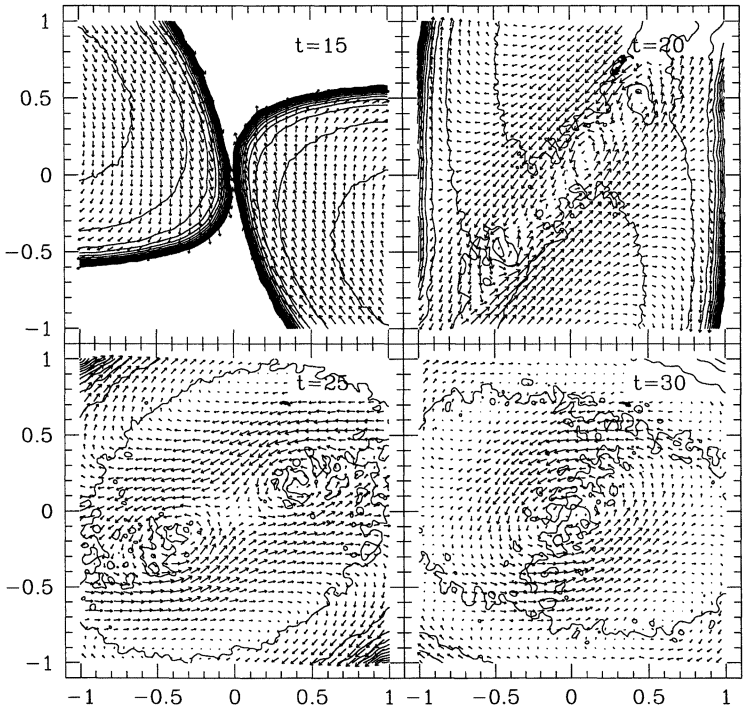

FIGURE 2. Density contours and velocities along the equatorial plane in the corotating frame of the binary, for the same times as in Fig. 1.

GRAVITY WAVE SIGNALS AND SPECTRA

We calculate the gravity wave signal for our mergers in the quadrupole approximation. The gravity wave strain h seen by an observer located a distance d from the center of mass of the system along the rotation axis is given for the two polarizations by

$$c^4(dh_+) = \ddot{Q}_{xx} - \ddot{Q}_{yy} \tag{1}$$

$$c^4(dh_\times) = 2\ddot{Q}_{xy} \tag{2}$$

where $\ddot{Q}$, the second time derivative of the quadrupole moment tensor, is given in SPH terms by

$$\ddot{Q}_{ij} = \sum_b m_b(v_i^{(b)}v_j^{(b)} + x_i^{(b)}\dot{v}_j^{(b)} + x_j^{(b)}\dot{v}_i^{(b)}) \tag{3}$$

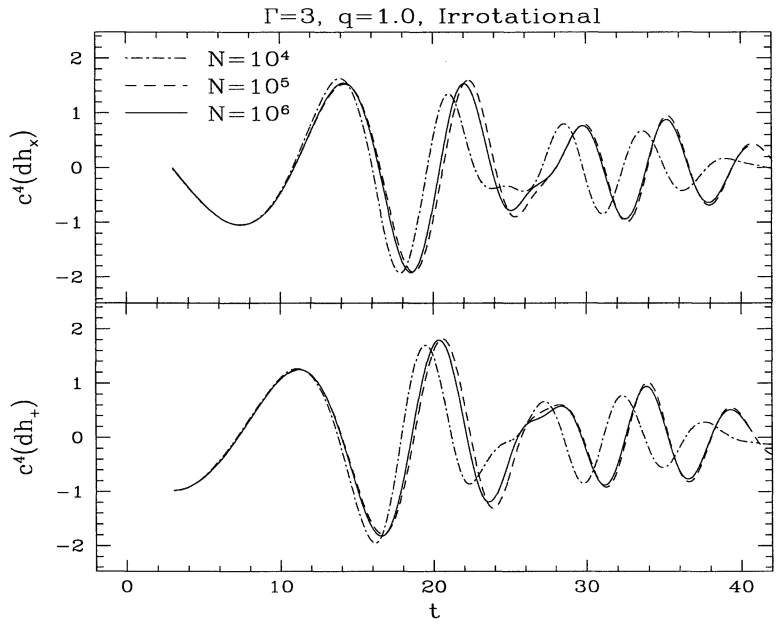

FIGURE 3. Gravity wave signals calculated for coalescences with the same initial parameters but different numerical resolutions. The solid, dashed, and dot-dashed lines correspond to runs with 10^6, 10^5, and 10^4 SPH particles, respectively.

where the summation is taken over all the particles in the calculation. In Fig. 3, we show the gravity wave signals in both polarizations, h_+ and $h_\times$, for the irrotational run described above, as well as for runs with $N = 50,000$ particles and $N = 5,000$ particles per NS, calculated as described in [10]. It is immediately apparent that the lowest resolution run shows significant discrepancies from the other two, which agree with each other quite well over the entire time history of the merger. This is a welcome result, given that the vortex sheet appearing at the contact surface is Kelvin-Helmholtz unstable on all size scales, including those much smaller than our numerical resolution. Even though differences in the exact location and size of vortices were apparent for runs of differing resolution, we found that the paths traced out by the respective NS cores, which make up the dominant contribution to the GW signal, were almost identical. The conclusion to be drawn is that numerical convergence for a given set of initial conditions and physical assumptions is possible without requiring excessive computational resources, even for this difficult problem involving small-scale instabilities.

ACKNOWLEDGMENTS

This work was supported in part by NSF Grants AST-9618116 and PHY-0070918 and NASA ATP Grant NAG5-8460. The computations were supported by the National Computational Science Alliance under grant AST980014N and utilized the NCSA SGI/CRAY Origin2000.

REFERENCES

1. Faber, J.A., Rasio, F.A., and Manor, J.B., *Phys. Rev. D* **63**, 044012 (2001).
2. Rasio, F.A., and Shapiro, S.L., *Class. Quant. Grav.* **16**, R1-R29 (1999).
3. Oohara, K., and Nakamura, T., *Prog. Theor. Phys.* **82**, 535-554 (1989); *ibid.* **83**, 906-940 (1990); Nakamura, T. and Oohara, K., *ibid.* **82**, 1066-1083 (1989); *ibid.* **86**, 73-88 (1991).
4. Shibata, M., Oohara, K., and Nakamura, T., *Prog. Theor. Phys.* **88**, 1079-1095 (1992); *ibid.* **89**, 809-819 (1993).
5. New, K.C.B., and Tohline, J.E., *Astrophys. J.* **490**, 311-327 (1997).
6. Swesty, F.D., Wang, E.Y.M., and Calder, A.C., *Astrophys. J.* **541**, 937-958 (2000).
7. Ruffert, M., Janka, H.-Th., and Schäfer, G., *Astron. Astrophys.* **311**, 532-566 (1996).
8. Ruffert, M., Janka, H.-Th., Takahashi, K., and Schäfer, G., *Astron. Astrophys.* **319**, 122-153 (1997).
9. Ruffert, M., Rampp, M., and Janka, H.-Th., *Astron. Astrophys.* **321**, 991-1006 (1997).
10. Rasio, F.A., and Shapiro, S.L., *Astrophys. J.* **401**, 226-245 (1992); *ibid.* **432**, 242-261 (1994); *ibid.* **438**, 887-903 (1995).
11. Zhuge, X., Centrella, J., and McMillan, S., *Phys. Rev. D* **50**, 6247-6261 (1994); *ibid.* **54**, 7261-7277 (1996).
12. Davies, M.B. et al., *Astrophys. J.* **431**, 742-753 (1994).
13. Rosswog, S. et al., *Astron. Astrophys.* **341**, 499-526 (1999).
14. Rosswog, S. et al., *Astron. Astrophys.* **360**, 171-184 (2000).
15. Baumgarte, T.W., Hughes, S.A., and Shapiro, S.L., *Phys. Rev. D.* **60**, 087501 (1999); Shibata, M., *Phys. Rev. D* **60**, 104052 (1999).
16. Faber, J.A. and Rasio, F.A., *Phys Rev. D* **62**, 064012 (2000).
17. Ayal, S. et al., *Astrophys. J.*, accepted, astro-ph/9910154.
18. Blanchet, L., Damour, T., and Schäfer, G., *Mon. Not. Roy. Astron. Soc.* **242**, 289-305 (1990).
19. Bildsten, L., and Cutler, C., *Astrophys. J.* **400**, 175-180 (1992).
20. Lombardi, J.C., Rasio, F.A., and Shapiro, S.L., *Phys. Rev. D* **56**, 3416-3438 (1997).